THE JOURNAL OF PHYSICAL CHEMISTRY LETTERS
A JOURNAL OF THE AMERICAN CHEMICAL SOCIETY

pubs.acs.org/JPCL Letter

High-Harmonic Generation and Femtosecond-Resolved Ultrafast Dynamics in Liquid Water

Jiyu Xu* and Sheng Meng*

Cite This: *J. Phys. Chem. Lett.* 2025, 16, 5295−5301 Read Online

ACCESS | Metrics & More | Article Recommendations | Supporting Information

ABSTRACT: The high-harmonic generation (HHG) is of great significance for attosecond science, ultrafast detection, and control of quantum processes. Compared with gases and solids currently under extensive investigations, HHG from liquids is rarely studied, but it enables unique electron scattering processes different from those in gases and solids owing to the dense configuration without long-range order in liquids. Here using state-of-the-art *ab initio* quantum dynamics simulations, we investigated HHG in liquid water across a wide range of laser intensities. We identified the transition from isolated molecule behavior to condensed-phase dynamics and revealed the suppression of HHG due to ultrafast water plasma generation. This transition results in a scaling behavior of $E_0^{1.8}$ for cutoff energy E_c with respect to field strength E_0 of driving pulses before severe water dissociation. Further increasing field strength E_0 leads to ultrafast water dissociation and plasma generation, and in turn the enhanced decoherence and decrease of E_c. Via frequency filtering, the individual attosecond pulses can be obtained from liquid water. More importantly, photoinduced plasma generation and insulator-to-metal transition can be directly tracked via time-resolved HHG with femtosecond resolution. Our work offers novel insights into liquid-based HHG and reveals the femtosecond-resolved nonequilibrium dynamics of photoexcited liquid water, which can be experimentally probed by time-resolved HHG.

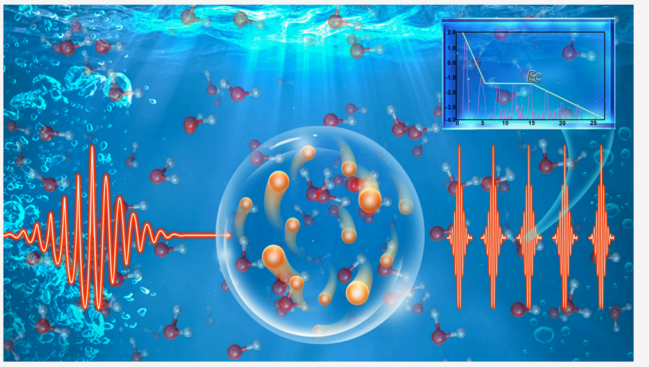

The high-harmonic generation (HHG) has been extensively studied in gaseous and solid systems owing to the great significances in attosecond science, ultrafast detection and coherent light sources.[1−5] The semiclassical three-step model (TSM) describing HHG in terms of electron trajectories accounts well for HHG in gaseous systems,[6] where the electron encounters the processes including tunnel ionization, acceleration and recombination with parent ions. The HHG of solids is attributed to the photoinduced intraband and interband currents, as a consequence of the formation of periodic lattice and electronic band structure.[7−10] The HHG spectra of solids exhibit unique characteristics, e.g., linear scaling of the cutoff energy E_c with the driving field strength,[11] anisotropic HHG generation,[12] ellipticity dependence,[7,13] noninteger high-harmonic generation,[14] etc. As the intermediate states between gases and solids, liquid systems exhibit dense configurations without long-range orders, delicate intermolecular interactions, and fluctuations in coordination, which could enable unique nonlinear electron dynamics under laser irradiation.

However, the exploration of HHG in liquids is scarce due to the experimental difficulties of distinguishing the contribution of bulk liquid and surrounding gaseous molecules.[15] Early experimental studies usually focused on the HHG from exploding water droplets.[16−18] Recent experiments measured the HHG spectra of pure liquid water via the liquid flat microjet technology,[15,19] where the obtained E_c of liquid water is 14.2 eV independent of wavelengths of driving pulses beyond an intensity threshold.[19] Theoretically, the model calculation of HHG of liquids lacks the realistic atomistic details and accurate electronic structures,[20] and direct first-principles simulations of liquid water suffer from the huge computational costs.[19,21] A detailed study of the intensity scaling of HHG is still lacking for liquid water. More importantly, the extreme nonlinearities essentially enable the high sensitivity of HHG to the changes of band structure and structural deformation,[22−24] which are usually neglected in previous studies of liquid HHG.[19]

In this work, we study the HHG spectrum and ultrafast dynamics of liquid water following photoexcitation employing *ab initio* real-time time-dependent density functional theory (rt-TDDFT) simulations. The rt-TDDFT naturally includes the photoinduced electronic excitations and the electron−electron and electron−ion scattering in dense amorphous configurations

Received: February 3, 2025
Revised: May 14, 2025
Accepted: May 16, 2025
Published: May 20, 2025

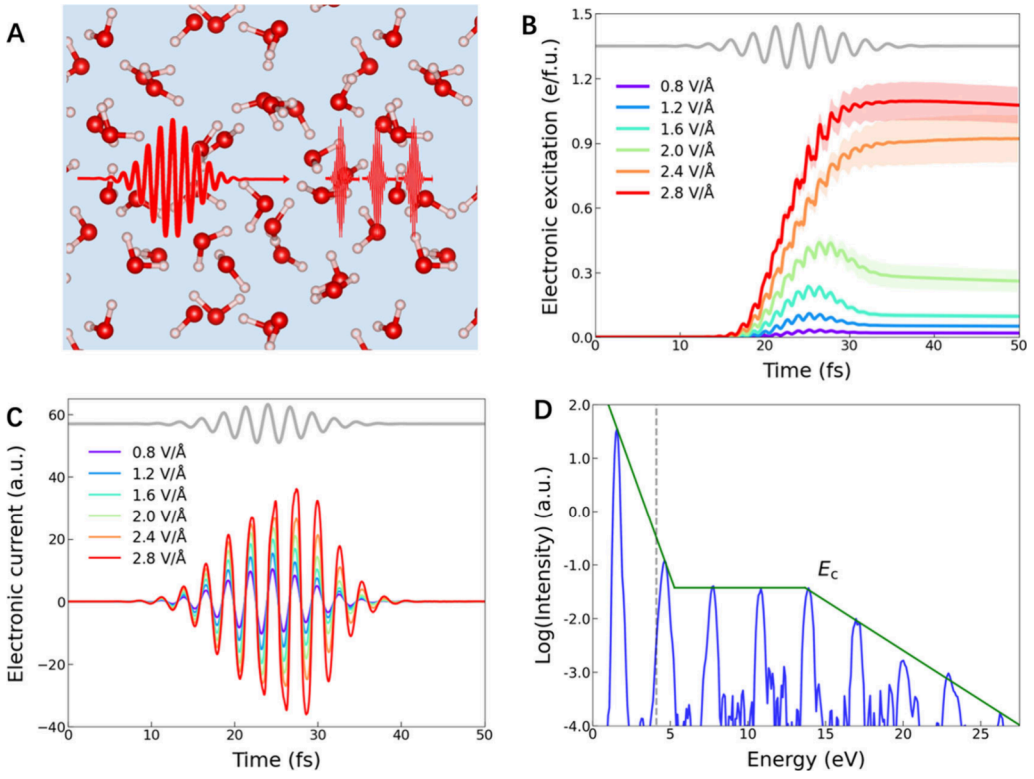

Figure 1. Photoinduced ultrafast nonequilibrium dynamics and HHG of liquid water. (A) The schematic of HHG in liquid water. (B) The electronic excitation as a function of E_0 of 800 nm laser pulses. The shaded areas indicate the standard error for each E_0. The envelope of the laser is also shown. (C) The electronic current as a function of E_0 of 800 nm laser pulses. (D) The simulated HHG spectrum for E_0 = 1.6 V/Å. The cutoff energy E_c is obtained with the intersection between the line of averaged harmonics in the plateau region and the linear fit in the exponential decayed cutoff region. The dotted line indicates the calculated bandgap of liquid water.

and can predict the nonlinear electronic/nuclear dynamics and high harmonic emissions of liquid water (Figure 1A). The HHG spectra of liquid water are shown to have E_c values reaching the extreme ultraviolet (XUV) regime. The transition from isolated molecular behavior to condensed-phase dynamics is revealed, in good agreement with semiclassical analysis. This transition results in a scaling relationship of $E_0^{1.8}$ for E_c with respect to the electric field strength E_0 of driving lasers before severe water dissociations take place. The time-resolved analysis of HHG can directly track the photoinduced water plasma generation and insulator-to-metal transition (IMT) with a femtosecond resolution. Plasma generation and IMT decrease both E_c and intensity of high-order harmonics and simultaneously enhance the decoherence of HHG in both frequency and time domain. The individual attosecond pulse can be obtained via frequency filtering from liquid water without severe water dissociation.

The rt-TDDFT simulations were performed with the TDAP[25,26] code as implemented in Quantum Espresso.[27] We employed the optimized norm-conserving Vanderbilt (ONCV) pseudopotentials[28] and the optB88-vdW van der Waals density functional.[29] The energy cutoff of 85 Ry was used in all simulations. The liquid water was represented with a periodic 32-water-molecule cubic cell with a density of 1 g/cm^3. The time step for nuclei motion is 0.05 fs, and the time step for electron evolution is 0.1 as. The simulation setups were similar to those used in our previous study.[30] The liquid water was first equilibrated for 50 ps in the constant-volume and constant-temperature (NVT) ensemble, and 30 representative configurations were extracted every 1 ps from the last 30 ps simulation. The obtained configurations were then excited with the laser pulses of $E(t) = E_0 \cos(\omega t) \exp[-(t - t_0)^2/2\sigma^2]$. The laser wavelength λ = 800 nm was used with the pulse width σ = 5 fs centered at t_0 = 24 fs. The photon energy of 1.55 eV is less than both the calculated and experimental band gaps of liquid water.[31] The electric field strength E_0 ranges from 0.8 to 2.8 V/Å. The detailed simulation methods can be found in the Methods section.

Upon photoexcitation, the valence electrons of liquid water are promoted to the conduction band. Figure 1B shows the temporal evolution of photoinduced electronic excitation of liquid water, which is averaged on 30 trajectories for each E_0. The maximum density of electronic excitation is ~0.2 e/f.u. for E_0 = 1.6 V/Å and reaches ~1 e/f.u. for E_0 = 2.4 V/Å (Figure S1). As shown in Figure 1C, the oscillating laser field drives the electric currents periodically in liquid water. Here the time-dependent electronic current is calculated as $\boldsymbol{j}(t) = \sum_{lk} \frac{1}{2i} \int dr[\psi_{lk}^*(r, t)\nabla\psi_{lk}(r, t) + c.c.]$. The currents perpendicular to electric field direction are negligible owing to the isotropy of liquid water and the statistical averages of 30 trajectories for each E_0 (Figure S2). The origin of electronic currents can be attributed to the intraband and interband contributions, owing to the dense configurations of liquid systems like those in crystalline materials.

The HHG spectrum of liquid water is obtained via the Fourier transform of the derivative of electronic current along electric field direction as $HHG(\omega) = \left|\int \frac{\partial}{\partial t} j(t) \exp(-i\omega t) dt\right|^2$. Figure 1D shows the HHG spectrum with a laser irradiation of E_0 = 1.6 V/Å. Obvious odd harmonics are obtained, reflecting the inversion symmetry of amorphous liquid systems. The intensity

https://doi.org/10.1021/acs.jpclett.5c00353
J. Phys. Chem. Lett. 2025, 16, 5295−5301

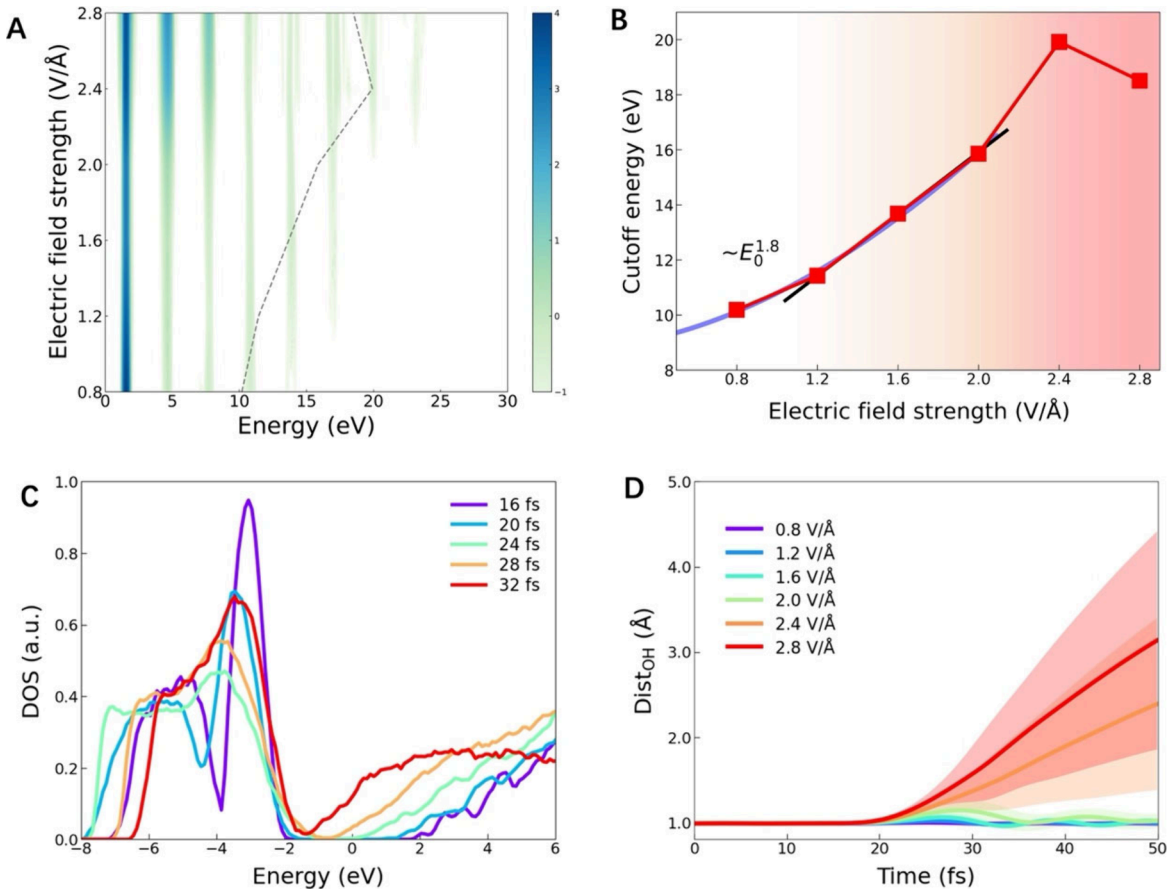

Figure 2. HHG spectrum of liquid water and water plasma. (A) The HHG spectra as a function of E_0 of driving pulses. The HHG spectra are shifted with plateau regions to zero for all E_0. E_c is also shown in the figure. (B) E_c as a function of E_0 of 800 nm laser pulses. The two fitted lines are also shown. (C) The temporal evolutions of electronic density of states of water with E_0 = 2.4 V/Å. (D) The temporal evolutions of the distances between oxygen and hydrogen atoms in initial water molecules. The shaded areas indicate the standard errors.

of the 15th harmonic (of the 800 nm fundamental wavelength) is greater than the noise signals perpendicular to the electric field direction (Figure S3A). Thus, the effective harmonic extends beyond 20 eV, consistent with experimental measurements.[15] The cutoff energy E_c is defined as the intersection between the fitted line of averaged harmonics in the plateau region and the linear fit in the exponential decayed cutoff region. The obtained E_c of ∼13.7 eV is in the XUV regime, and it is close to the experimental measurements of 14.2 eV for liquid water.[19] The entrance energy E_{enter} of the plateau region is slightly greater than the calculated bandgap of ∼4.1 eV of liquid water.

Figure 2A and Figure S4 exhibit the shifted and original HHG spectra as a function of E_0 of 800 nm laser pulses, respectively. The magnitude of harmonics basically increases with the E_0 of driving pulses (Figure S4), while the peaks of high-order harmonics are gradually blurred and incoherent for E_0 > 2.4 V/Å (Figure 2A). The individual HHG spectrum for each E_0 is shown in Figure S5, and E_c can be extracted from the intersection of fitting lines. E_c is beyond 10 eV for all E_0 values and lies in the XUV regime. Besides, E_c increases with E_0 for E_0 < 2.4 V/Å and then decreases as shown in Figure 2B. The maximum of E_c is ∼20 eV for E_0 = 2.4 V/Å. The fitted E_{enter} is ∼5 eV for E_0 < 1.6 eV and increases up to ∼11 eV for E_0 = 2.8 eV (Figure S4).

A detailed analysis reveals a linear relationship between E_c and E_0 within the regime of 1.2 V/Å < E_0 < 2.0 V/Å, consistent with the extended semiclassical analysis.[19] The deviation observed at E_0 = 0.8 V/Å reflects the nature of HHG of isolated molecules under weak laser irradiations.[6] Consequently, E_c is proportional to $E_0^{1.8}$ for laser pulses with E_0 < 2.0 V/Å. The experimental measurements of ellipticity dependence also demonstrate the similarity of HHG spectra between gas molecules and liquids as well,[15] while the ellipticity dependence of HHG is complex in solids due to anisotropic electronic structures.[7,13] We note that the expansion of liquid leads to the higher efficiency of high harmonic emissions and the increase of E_c,[18,19] and here the effects of density variations are excluded in constant-volume simulations.

E_c decreases with E_0 for laser pulses with E_0 > 2.4 V/Å, reflecting the photoinduced variations of electronic structure. A previous study demonstrates that metallic water plasma can be generated for laser irradiation with E_0 > 2.2 V/Å.[30] Figure 2C illustrates the temporal evolution of the electronic density of states during laser irradiation with E_0 = 2.4 V/Å, and the transition from an insulator to a metal is observed. The distances between oxygen and hydrogen atoms of original molecules suddenly increase upon photoexcitation, as shown in Figure 2D, corresponding to the severe water dissociation (Figure S6). Here, IMT leads to the suppression of high-order harmonics and the decrease of E_c owing to the essentially linear response and screening effects of free electrons in metallic systems.[22,32,33] The decrease of E_c is demonstrated for photoexcited water droplets under intense laser irradiations.[18] Experimental study also demonstrates that E_c of water plasma still lies in this region even under the coherent wake emission (CWE) mechanism.[34,35]

https://doi.org/10.1021/acs.jpclett.5c00353
J. Phys. Chem. Lett. 2025, 16, 5295−5301

Figure 3 presents the intensity of individual harmonics relative to E_0 of laser pulses on a double logarithmic scale. The 3rd harmonic (of the 800 nm fundamental wavelength) exhibits a power dependence of ~5.9 with E_0 in the perturbative region.

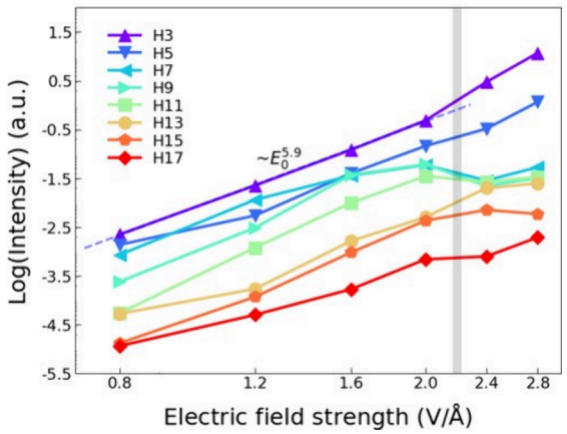

Figure 3. Dependence of the intensity of an individual harmonic on E_0 of laser pulses on a double logarithmic scale. The dotted fitted line shows the perturbative behavior of the 3rd harmonic (of the 800 nm fundamental wavelength). Higher orders are all in the nonperturbative regions. The thick gray line indicates the transition to water plasma emission, and the scaling deviates from the extrapolation at lower intensity.

Higher harmonics all fall in the nonperturbative region, displaying similar power dependencies for E_0 < 2.0 V/Å. For E_0 > 2.4 V/Å, the metallic plasma generation leads to the deviation from the extrapolation of lower laser intensity. Especially, the power of the 3rd harmonic increases to ~8.9, indicating the appearance of multiple processes involving both plasma generation and HHG emission. The intensities of the 7th, 11th and 13th harmonics decrease during generation of photoinduced water plasma, and the decreases may be attributed to enhanced electron−ion scatterings and screening effects originating from IMT.[32,33] The peaks of these harmonics are all blurred in the HHG spectra of water plasma for E_0 > 2.4 V/Å (Figure 2A and Figure S5). Moreover, the high harmonics emitted perpendicular to the laser direction are nearly comparable to those along the laser direction, reflecting the random and incoherent laser emission of water plasma (Figure S3B).

To directly illustrate the HHG emission, we performed the time-resolved analysis of the HHG spectrum via wavelet transform with a complex Morlet wavelet. Figure S7A and Figure 4A show the time-resolved HHG spectra with laser intensity of 0.8 and 1.2 V/Å, respectively. The femtosecond resolution of HHG spectra is achieved. The emergence of a frequency chip demonstrates the crucial contribution of interband currents to high harmonic emissions,[36] resembling the recombination emissions in gaseous molecules.[6] It demonstrates the finite movements of tunneling electrons and the independence of individual water molecules, which accounts

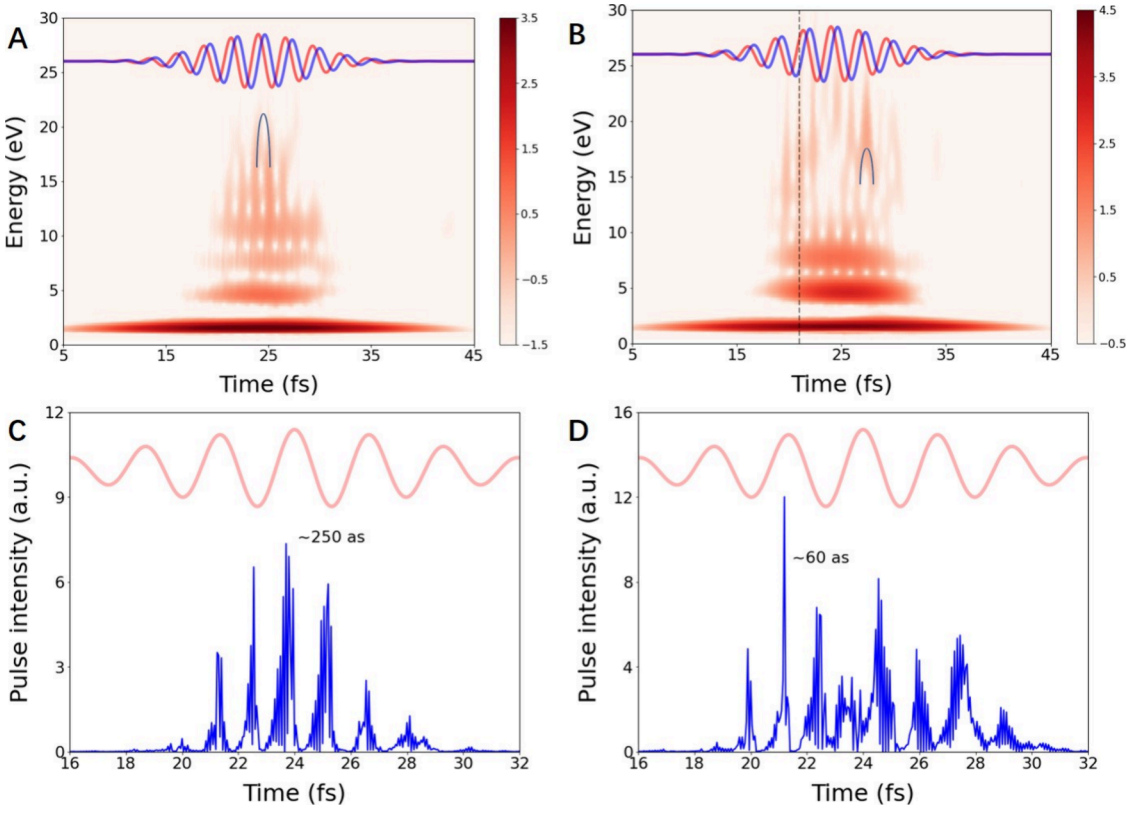

Figure 4. Time-resolved analysis of the HHG spectrum and the emission of attosecond pulse trains. The time-resolved HHG spectra with E_0 of 1.2 V/Å (A) and 2.4 V/Å (B). The red and blue lines indicate the electric field E_z and vector potential A_z of laser pulses, respectively. The arcs illustrate the frequency chirp contributed by interband currents. The dotted line shows the emission of harmonics by the coupled interband and intraband currents. The emission of attosecond pulse trains for E_0 of 2.0 V/Å (C) and 2.4 V/Å (D). The frequency beyond 20 eV is filtered to generate the attosecond pulse trains.

https://doi.org/10.1021/acs.jpclett.5c00353
J. Phys. Chem. Lett. 2025, 16, 5295−5301

for the similarities between the HHG of liquid water and those of gaseous molecules under weak laser irradiations. From a semiclassical perspective, all ejected electrons are expected to contribute to the HHG spectrum in the weak laser intensity regime. A similar phenomenon is also demonstrated in HHG of two-dimensional materials with laser polarization directions perpendicular to the material plane.[37]

The increase of laser intensity leads to stronger electronic excitations and longer movements of the photocarrier, and meanwhile, the contributions of intraband currents are also enhanced. Figure S7B,C exhibits the time-resolved HHG spectra of E_0 = 1.6 and 2.0 V/Å, respectively. One can see that the emission of high harmonics takes place every half laser cycle and at the times between the maximum of electric field and that of vector potential. The coupled interband and intraband currents contribute to the emissions of high harmonics, which is similar to the complex interplay of intraband and interband currents to HHG in bulk solids.[7,8,38−40] Semiclassical analysis shows that the short electron trajectories alone account for the dependence of E_c in this intensity regime.[19] Since all electron trajectories are included in rt-TDDFT simulations, these results demonstrate that the inclusion of long electron trajectories does not affect E_c.

The intense laser-induced water plasma generation and IMT can be directly monitored with time-resolved HHG owing to the femtosecond resolution. Figure 4B and Figure S7D show the time-resolved HHG spectra of E_0 = 2.4 and 2.8 V/Å, respectively. For E_0 = 2.4 V/Å, the time-resolved harmonic emissions from t = 18 fs to t = 23 fs resemble those of E_0 = 1.6 and 2.0 V/Å, reflecting the similar insulating electronic states (Figure 2C). A depletion of HHG emissions is observed from t = 23 fs to t = 25 fs, which coincides with the decrease of bandgap as shown in Figure 2C. From t = 25 fs to t = 29 fs, the emergence of frequency chirp demonstrates the dominance of interband currents for the water plasma. The enhancement of interband currents is attributed to the large photocarrier densities (Figure 1B). The mechanism variations for HHG emissions result in the decoherence of the HHG spectrum in Figure 2A. Nevertheless, it also demonstrates that the time-resolved HHG spectrum can be employed to monitor the optically driven femtosecond electronic phase transitions.[22,32,33]

Based on the above analysis, a comprehensive description of the intensity dependence of E_c and HHG spectra can be established. In the weak laser intensity regime, the electric field induces only finite electron excursions, and all electron trajectories contribute to the HHG spectra as described by the conventional TSM.[6] As the laser intensity increases, electron scattering takes place and multiple current contributions account for the HHG emissions. A linear relationship between E_c and E_0 is obtained, with short electron trajectories dominating the HHG spectra as shown in extended semiclassical analysis.[19] Under intense laser irradiations, the water plasma generation and IMT take place in liquid water.[30] The resulting metallization leads to enhanced decoherence and a decrease of E_c owing to the linear response and screening effects of free electrons. It should be noted that the weak linear scaling between E_c and E_0 in extended semiclassical analysis assumes an exclusive contribution from short electron trajectories.[19] In practice, both short and long electron trajectories contribute to HHG spectra under weak laser intensities.

Owing to E_c being over 10 eV, the HHG from liquid water is capable of generating the attosecond pulses in the XUV regime. The attosecond pulse trains can be directly simulated using inverse Fourier transform with frequency filtering. Here, the frequency beyond 20 eV is filtered to generate the pulse trains, mimicking the filtering processes of aluminum membranes. The predicted attosecond pulse train with the HHG spectrum of E_0 = 2.0 V/Å is shown in Figure 4C. The coherent attosecond pulses in the XUV region are emitted every half laser cycle. The emitted pulses have an average duration of ∼250 as with its peak intensity located between the maximum of electric field and that of vector potential, consistent with the time-resolved HHG spectrum in Figure S7C. On the contrary, the generation of attosecond pulses with E_0 = 2.4 V/Å is complex due to the multiple processes of plasma generation (Figure 4D). The initial attosecond pulses are roughly isolated, and even the ultrashort duration of ∼60 as is achieved in the second pulse. The intensities of middle pulses gradually decrease, and the later pulses are not well separated. These characteristics of attosecond pulses are well consistent with the time-resolved HHG spectrum. Therefore, the plasma generation lowers the efficiency of attosecond pulse generation, and the ultrashort attosecond pulse can only be generated in liquid water without severe water dissociation.

In conclusion, we have studied the HHG spectrum and the ultrafast dynamics of photoexcited liquid water. The oscillating laser fields drive the electronic currents periodically, and the obtained HHG spectra of liquid water have E_c in the XUV regime. Due to the transition from isolated molecule behavior to condensed-phase dynamics, E_c is found to be proportional to $E_0^{1.8}$ for liquid water before severe water dissociation. The time-resolved analysis reveals that the coupled intraband and interband currents contribute the harmonics in the non-perturbative region of liquid water. Besides, the plasma generation and IMT can be directly monitored with time-resolved HHG with femtosecond resolution. The water plasma generation decreases both E_c and the intensity of high-order harmonics. Besides, the water plasma generation enhances the decoherence of the HHG spectrum in both frequency and time domains, and the ultrashort attosecond pulse can only be generated in liquid water without severe water dissociation.

METHODS

The photoinduced nonequilibrium dynamics of liquid water were simulated via the rt-TDDFT algorithm TDAP[25,26] as implemented in Quantum Espresso.[27] We used the optimized norm-conserving Vanderbilt (ONCV) pseudopotentials[28] and the van der Waals density functional with the optB88-vdW method.[29] The energy cutoff was set to 85 Ry in all of the simulations. The liquid water was simulated with a periodic 32-water-molecule cubic cell, and the density is 1 g/cm^3. Despite that a denser k-point mesh describes well the delocalized conduction states, a 2 × 2 × 2 k-point mesh is used to sample the Brillouin zone and is shown to give the reasonable HHG spectra (Figure S8A). The convergence tests with a 64-water-molecule model also demonstrate the reliability of this model (Figure S9). The calculated band gap of liquid water is ∼4.1 eV, consistent with the GGA results of 4.36 eV.[31] It is worth noting that underestimation of bandgap may lead to a systematic underestimation of E_c.[19] Additional 52 unoccupied electronic states were considered in the nonadiabatic simulations. The time step of nuclear movement is 0.05 fs, and the time step of electron evolutions is 0.1 as. A total 50 fs of simulation was performed for each trajectory. The similar setups were shown to describe well the ultrafast dynamics of liquid water.[30]

https://doi.org/10.1021/acs.jpclett.5c00353
J. Phys. Chem. Lett. 2025, 16, 5295−5301

Ab initio molecular dynamics simulations were performed to equilibrate the properties of liquid water using Quantum Espresso.[27] The equilibrium simulation with a time step of 1 fs was performed for 50 ps at 300 K in the NVT ensemble, and the Berendsen thermostat is used with the time parameter of 200 fs. The representative configurations were extracted every 1 ps from the last 30 ps of simulation, and 30 configurations of liquid water were obtained. The long-time ground-state simulations are necessary to sample the phase space and to describe well coordination fluctuations of liquid water (Figure S8B). The obtained configuration was then irradiated with laser pulses of $E(t) = E_0 \cos(\omega t) \exp[-(t-t_0)^2/2\sigma^2]$. We chose the laser pulses with wavelength $\lambda = 800$ nm and the width $\sigma = 5$ fs centered at $t_0 = 24$ fs. The photon energy of 1.55 eV is less than both the calculated and experimental band gaps of liquid water;[31] thus the photoexcitation mechanisms are unchanged. The electric field E_0 ranges from 0.8 to 2.8 V/Å. The velocity gauge is used to enable periodic electric fields in simulations. Total 240 rt-TDDFT trajectories were simulated to systematically study the intensity scaling of HHG and ultrafast dynamics of photoexcited liquid water. More accurate setups were used to study the wavelength-dependent HHG spectrum and predict well the wavelength-independence of E_c in liquid systems.[19] Given that phase transitions induce significant changes in atomistic configurations and electronic structures and that a wide range of laser intensities is considered in our calculations, the simplified model used here can still provide a reasonable description of HHG in liquid water owing to the obvious changes of HHG (Figure S4).

The HHG spectrum was obtained with Fourier transform of the derivative of time-dependent electronic current $j(t)$ as $HHG(\omega) = \left|\int \frac{\partial}{\partial t} j(t) \exp(-i\omega t) dt\right|^2$, and only electronic current along the electric field direction is used. The time-dependent electronic current is calculated as $\boldsymbol{j}(t) = \sum_{lk} \frac{1}{2i} \int dr[\psi_{lk}^*(r,t) \nabla \psi_{lk}(r,t) + c.c.]$. The time-resolved HHG spectrum was retracted via the continuous wavelet transform (CWT) as $HHG(\omega, t) = \left|\int \frac{\partial}{\partial t} j(t') \frac{1}{\sqrt{\omega}} \Psi^*\left(\frac{t'-t}{\omega}\right) dt'\right|^2$, and the complex Morlet wavelet is used as the mother wavelet Ψ. The frequency filtering is employed to obtain the attosecond pulse trains, $E(t) = \int_{\omega_0}^{\infty} \exp(i\omega t) d\omega \int \frac{\partial}{\partial t} j(t') \exp(-i\omega t') dt'$, and ω_0 is chosen as 20 eV to approximately simulate the filtering process of the aluminum membrane in experiments.

■ ASSOCIATED CONTENT

Data Availability Statement

The data that support the findings of this study are available from the corresponding author upon reasonable request.

Supporting Information

The Supporting Information is available free of charge at https://pubs.acs.org/doi/10.1021/acs.jpclett.5c00353.

The electronic excitation with electric field strength of laser pulses, the anisotropic electronic currents and HHG spectra, the original HHG spectra with electric field strength, the atomistic configuration of water plasma, the time-resolved HHG spectra with electric field strength, and the convergence tests of *k*-points and lattice sizes (PDF)

Transparent Peer Review report available (PDF)

■ AUTHOR INFORMATION

Corresponding Authors

Jiyu Xu − *Institute of Physics, Chinese Academy of Sciences, Beijing 100190, China; Songshan Lake Materials Laboratory, Dongguan, Guangdong 523808, China;* orcid.org/0000-0002-2628-5492; Email: jiyuxu@iphy.ac.cn

Sheng Meng − *Institute of Physics, Chinese Academy of Sciences, Beijing 100190, China; Songshan Lake Materials Laboratory, Dongguan, Guangdong 523808, China;* orcid.org/0000-0002-1553-1432; Email: smeng@iphy.ac.cn

Complete contact information is available at: https://pubs.acs.org/10.1021/acs.jpclett.5c00353

Author Contributions

J.X. and S.M. conceived the project. J.X. designed the project and carried out the nonadiabatic rt-TDDFT simulations. J.X. analyzed the data. J.X. and S.M. discussed the results and wrote the paper.

Notes

The authors declare no competing financial interest.

■ ACKNOWLEDGMENTS

We acknowledge financial support from the National Natural Science Foundation of China (No. 12204513, No. 12025407 and No. 11934003), the Ministry of Science and Technology (No. 2021YFA1400201), Chinese Academy of Sciences (No. XDB33030100 and No. YSBR047) and Guangdong Basic and Applied Basic Research Foundation (No. 2023B1515120042).

■ REFERENCES

(1) Ghimire, S.; Reis, D. A. High-harmonic generation from solids. *Nat. Phys.* **2019**, *15*, 10−16.

(2) Goulielmakis, E.; Brabec, T. High harmonic generation in condensed matter. *Nat. Photonics* **2022**, *16*, 411−421.

(3) Winterfeldt, C.; Spielmann, C.; Gerber, G. Colloquium: Optimal control of high-harmonic generation. *Rev. Mod. Phys.* **2008**, *80*, 117−140.

(4) Li, J.; Lu, J.; Chew, A.; Han, S.; Li, J.; Wu, Y.; Wang, H.; Ghimire, S.; Chang, Z. Attosecond science based on high harmonic generation from gases and solids. *Nat. Commun.* **2020**, *11*, 2748.

(5) Weissenbilder, R.; Carlström, S.; Rego, L.; Guo, C.; Heyl, C. M.; Smorenburg, P.; Constant, E.; Arnold, C. L.; L'Huillier, A. How to optimize high-order harmonic generation in gases. *Nat. Rev. Phys.* **2022**, *4*, 713−722.

(6) Corkum, P. B. Plasma perspective on strong field multiphoton ionization. *Phys. Rev. Lett.* **1993**, *71*, 1994−1997.

(7) Tancogne-Dejean, N.; Mucke, O. D.; Kartner, F. X.; Rubio, A. Ellipticity dependence of high-harmonic generation in solids originating from coupled intraband and interband dynamics. *Nat. Commun.* **2017**, *8*, 745.

(8) Garg, M.; Zhan, M.; Luu, T. T.; Lakhotia, H.; Klostermann, T.; Guggenmos, A.; Goulielmakis, E. Multi-petahertz electronic metrology. *Nature* **2016**, *538*, 359−363.

(9) Vampa, G.; Hammond, T. J.; Thiré, N.; Schmidt, B. E.; Légaré, F.; McDonald, C. R.; Brabec, T.; Corkum, P. B. Linking high harmonics from gases and solids. *Nature* **2015**, *522*, 462−464.

(10) Luu, T. T.; Garg, M.; Kruchinin, S. Yu.; Moulet, A.; Hassan, M. Th.; Goulielmakis, E. Extreme ultraviolet high-harmonic spectroscopy of solids. *Nature* **2015**, *521*, 498−502.

(11) Ghimire, S.; DiChiara, A. D.; Sistrunk, E.; Agostini, P.; DiMauro, L. F.; Reis, D. A. Observation of high-order harmonic generation in a bulk crystal. *Nat. Phys.* **2011**, *7*, 138−141.

(12) You, Y. S.; Reis, D. A.; Ghimire, S. Anisotropic high-harmonic generation in bulk crystals. *Nat. Phys.* **2017**, *13*, 345−349.

(13) Yoshikawa, N.; Tamaya, T.; Tanaka, K. High-harmonic generation in graphene enhanced by elliptically polarized light excitation. *Science* **2017**, *356*, 736−738.
(14) Schmid, C. P.; Weigl, L.; Grössing, P.; Junk, V.; Gorini, C.; Schlauderer, S.; Ito, S.; Meierhofer, M.; Hofmann, N.; Afanasiev, D.; Crewse, J.; Kokh, K. A.; Tereshchenko, O. E.; Güdde, J.; Evers, F.; Wilhelm, J.; Richter, K.; Höfer, U.; Huber, R. Tunable non-integer high-harmonic generation in a topological insulator. *Nature* **2021**, *593*, 385−390.
(15) Luu, T. T.; Yin, Z.; Jain, A.; Gaumnitz, T.; Pertot, Y.; Ma, J.; Worner, H. J. Extreme−ultraviolet high−harmonic generation in liquids. *Nat. Commun.* **2018**, *9*, 3723.
(16) Kurz, H. G.; Kretschmar, M.; Binhammer, T.; Nagy, T.; Ristau, D.; Lein, M.; Morgner, U.; Kovacev, M. Revealing the Microscopic Real-Space Excursion of a Laser-Driven Electron. *Phys. Rev. X* **2016**, *6*, No. 031029.
(17) Flettner, A.; Pfeifer, T.; Walter, D.; Winterfeldt, C.; Spielmann, C.; Gerber, G. High-harmonic generation and plasma radiation from water microdroplets. *Appl. Phys. B: Laser Opt.* **2003**, *77*, 747−751.
(18) Kurz, H. G.; Steingrube, D. S.; Ristau, D.; Lein, M.; Morgner, U.; Kovacev, M. High-order-harmonic generation from dense water microdroplets. *Phys. Rev. A* **2013**, *87*, No. 063811.
(19) Mondal, A.; Neufeld, O.; Yin, Z.; Nourbakhsh, Z.; Svoboda, V.; Rubio, A.; Tancogne-Dejean, N.; Worner, H. J. High-harmonic spectroscopy of low-energy electron-scattering dynamics in liquids. *Nat. Phys.* **2023**, *19*, 1813−1820.
(20) Zeng, A.-W.; Bian, X.-B. Impact of Statistical Fluctuations on High Harmonic Generation in Liquids. *Phys. Rev. Lett.* **2020**, *124*, No. 203901.
(21) Neufeld, O.; Nourbakhsh, Z.; Tancogne-Dejean, N.; Rubio, A. Ab Initio Cluster Approach for High Harmonic Generation in Liquids. *J. Chem. Theory Comput.* **2022**, *18*, 4117−4126.
(22) Silva, R. E. F.; Blinov, I. V.; Rubtsov, A. N.; Smirnova, O.; Ivanov, M. High-harmonic spectroscopy of ultrafast many-body dynamics in strongly correlated systems. *Nat. Photonics* **2018**, *12*, 266−270.
(23) Bian, X.-B.; Bandrauk, A. D. Probing Nuclear Motion by Frequency Modulation of Molecular High-Order Harmonic Generation. *Phys. Rev. Lett.* **2014**, *113*, No. 193901.
(24) Neufeld, O.; Zhang, J.; De Giovannini, U.; Hubener, H.; Rubio, A. Probing phonon dynamics with multidimensional high harmonic carrier-envelope-phase spectroscopy. *Proc. Natl. Acad. Sci. U. S. A.* **2022**, *119*, No. e2204219119.
(25) Lian, C.; Zhang, S.-J.; Hu, S.-Q.; Guan, M.-X.; Meng, S. Ultrafast charge ordering by self-amplified exciton−phonon dynamics in TiSe2. *Nat. Commun.* **2020**, *11*, 43.
(26) Guan, M.; Chen, D.; Hu, S.; Zhao, H.; You, P.; Meng, S. Theoretical Insights into Ultrafast Dynamics in Quantum Materials. *Ultrafast Sci.* **2022**, *2022*, No. 9767251.
(27) Giannozzi, P.; et al. QUANTUM ESPRESSO: a modular and open-source software project for quantum simulations of materials. *J. Phys.: Condens.Matter* **2009**, *21*, No. 395502.
(28) Hamann, D. R. Optimized norm-conserving Vanderbilt pseudopotentials. *Phys. Rev. B* **2013**, *88*, No. 085117.
(29) Klimeš, J.; Bowler, D. R.; Michaelides, A. Chemical accuracy for the van der Waals density functional. *J. Phys.: Condens.Matter* **2010**, *22*, No. 022201.
(30) Xu, J.; Chen, D.; Meng, S. Probing Laser-Induced Plasma Generation in Liquid Water. *J. Am. Chem. Soc.* **2021**, *143*, 10382−10388.
(31) Chen, W.; Ambrosio, F.; Miceli, G.; Pasquarello, A. Ab initio Electronic Structure of Liquid Water. *Phys. Rev. Lett.* **2016**, *117*, No. 186401.
(32) Nie, Z.; Guery, L.; Molinero, E. B.; Juergens, P.; van den Hooven, T. J.; Wang, Y.; Jimenez Galan, A.; Planken, P. C. M.; Silva, R. E. F.; Kraus, P. M. Following the Nonthermal Phase Transition in Niobium Dioxide by Time-Resolved Harmonic Spectroscopy. *Phys. Rev. Lett.* **2023**, *131*, No. 243201.
(33) Bionta, M. R.; Haddad, E.; Leblanc, A.; Gruson, V.; Lassonde, P.; Ibrahim, H.; Chaillou, J.; Emond, N.; Otto, M. R.; Jimenez-Galan, A.; Silva, R. E. F.; Ivanov, M.; Siwick, B. J.; Chaker, M.; Legare, F. Tracking ultrafast solid-state dynamics using high harmonic spectroscopy. *Phys. Rev. Research* **2021**, *3*, No. 023250.
(34) Heissler, P.; et al. Using the third state of matter: high harmonic generation from liquid targets. *New J. Phys.* **2014**, *16*, No. 113045.
(35) Kim, Y. H.; Kim, H.; Park, S. C.; Kwon, Y.; Yeom, K.; Cho, W.; Kwon, T.; Yun, H.; Sung, J. H.; Lee, S. K.; Luu, T. T.; Nam, C. H.; Kim, K. T. High-harmonic generation from a flat liquid-sheet plasma mirror. *Nat. Commun.* **2023**, *14*, 2328.
(36) Wu, M.; Ghimire, S.; Reis, D. A.; Schafer, K. J.; Gaarde, M. B. High-harmonic generation from Bloch electrons in solids. *Phys. Rev. A* **2015**, *91*, No. 043839.
(37) Tancogne-Dejean, N.; Rubio, A. Atomic-like high-harmonic generation from two-dimensional materials. *Sci. Adv.* **2018**, *4*, No. eaao5207.
(38) Tancogne-Dejean, N.; Mucke, O. D.; Kartner, F. X.; Rubio, A. Impact of the Electronic Band Structure in High-Harmonic Generation Spectra of Solids. *Phys. Rev. Lett.* **2017**, *118*, No. 087403.
(39) Vampa, G.; McDonald, C. R.; Orlando, G.; Klug, D. D.; Corkum, P. B.; Brabec, T. Theoretical Analysis of High-Harmonic Generation in Solids. *Phys. Rev. Lett.* **2014**, *113*, No. 073901.
(40) Liu, H.; Li, Y.; You, Y. S.; Ghimire, S.; Heinz, T. F.; Reis, D. A. High-harmonic generation from an atomically thin semiconductor. *Nat. Phys.* **2017**, *13*, 262−265.

https://doi.org/10.1021/acs.jpclett.5c00353
J. Phys. Chem. Lett. 2025, 16, 5295−5301